

The affect of surface finish on the sliding wear of alumina

M. G. GEE, E. A. ALMOND

National Physical Laboratory, Teddington, Middlesex, UK

Two wear regimes were observed for a 95% alumina tested in dry sliding wear conditions using a pin on disc test geometry. Specimens prepared with lapped and polished surfaces exhibited low wear rates at applied loads of 10 and 40 N but ground surfaces wore rapidly at loads of 40 N and above. The surfaces that had experienced high wear rates contained more networks of microcracks and had rougher surface profiles than the mildly worn surfaces. X-ray line broadening analysis indicated that the wear debris had a particle size of 10 to 30 nm and contained plastic deformation, but no evidence of significant plastic deformation was found in the pin surfaces.

Theoretical explanations are proposed for the existence of two types of wear behaviour: subsurface crack growth is believed to cause high wear rates, whilst low wear rates are due to a very fine scale abrasion of the surface. Recommendations are made on some of the precautions that should be taken to use alumina successfully in dry sliding wear applications.

1. Introduction

A consequence of the improved properties of ceramics obtained by better processing and increased understanding of failure mechanisms, has been their introduction into applications where components are subjected to high static and dynamic loadings. For the latter, sustained transmission of load through a moving interface is almost inevitably accompanied by mechanical wear to the component or its counterface or to both. The extent of damage is affected by chemical reactions at or between the wear surfaces, and the degree of lubrication. The wear behaviour of individual ceramics is determined by the ease of plastic deformation relative to brittle fracture under the local stress conditions at the areas of contact at the wear interface. Since the initial and developed stress states are dependent on the surface profiles of the counterfaces, and on existing internal stresses and the chemical constitution of the surface layers it is evident that the initial surface preparation could have a considerable affect on wear mechanisms and wear rate. The work reported in this paper was directed towards clarifying the affect of surface preparation on the dry sliding wear characteristics of a 95% alumina tested in a pin on disc configuration.

2. Experimental method

2.1. Materials and apparatus

The tests were performed on a 5 μm grain size commercial 95% alumina in the form of 6 mm diameter by 30 mm long pins and 150 mm diameter by 10 mm thick discs. Specimens were prepared in three different ways: preparation A was to grind with a resin bonded wheel containing 100 to 200 μm grit diamond in a 50 to 75 vol % concentration, and to lap with 4 μm diamond on cast iron lap followed by polishing on a

copper-brass lap impregnated with 4 μm diamond. For preparation B the specimens were given the same grinding treatment as in A, but they were not lapped nor polished. Preparation C involved grinding with a metal bonded wheel containing 100 to 120 μm diamond in a 50 to 75% concentration. Identical preparations were given to the pin and the disc in each test. The edges of the pins were given a 0.5 mm wide 45° chamfer.

The layout of the wear testing apparatus is shown in Fig. 1. A counterweighted loaded arm was pivoted at large roller bearings at the rear of the machine. The loading arm had a 2:1 loading ratio with pivot to specimen distance of 210 mm and a loading point to pivot distance of 420 mm. Frictional forces acting on the pin were measured by a strain gauge load cell with a range of 0 to 250 N and a stiffness of $5.7 \times 10 \text{ MN m}^{-1}$, which protruded from a vertical pillar set at the side of the disc to arrest the horizontal movement of the loading arm. The combined wear of the pin and disc, expressed as the net vertical displacement between their surfaces, was measured by a linear variable differential transformer (LVDT) attached to the loading arm directly above the pin. The signals from both the friction load cell and LVDT were amplified by transducer conditioners, and could be filtered by low pass filters to remove any unwanted fluctuations in signal caused by residual misalignment of the test disc. The sensitivity of the displacement measurement system to changes in ambient temperature was $1.3 \times 10^{-6} \mu\text{m } ^\circ\text{C}^{-1}$.

2.2. Test procedure

The typical procedure for performing a test was to clamp the disc specimen to the support and orient the test surface perpendicular to the drive axis by fine adjustment of levelling screws. The top of the pin was

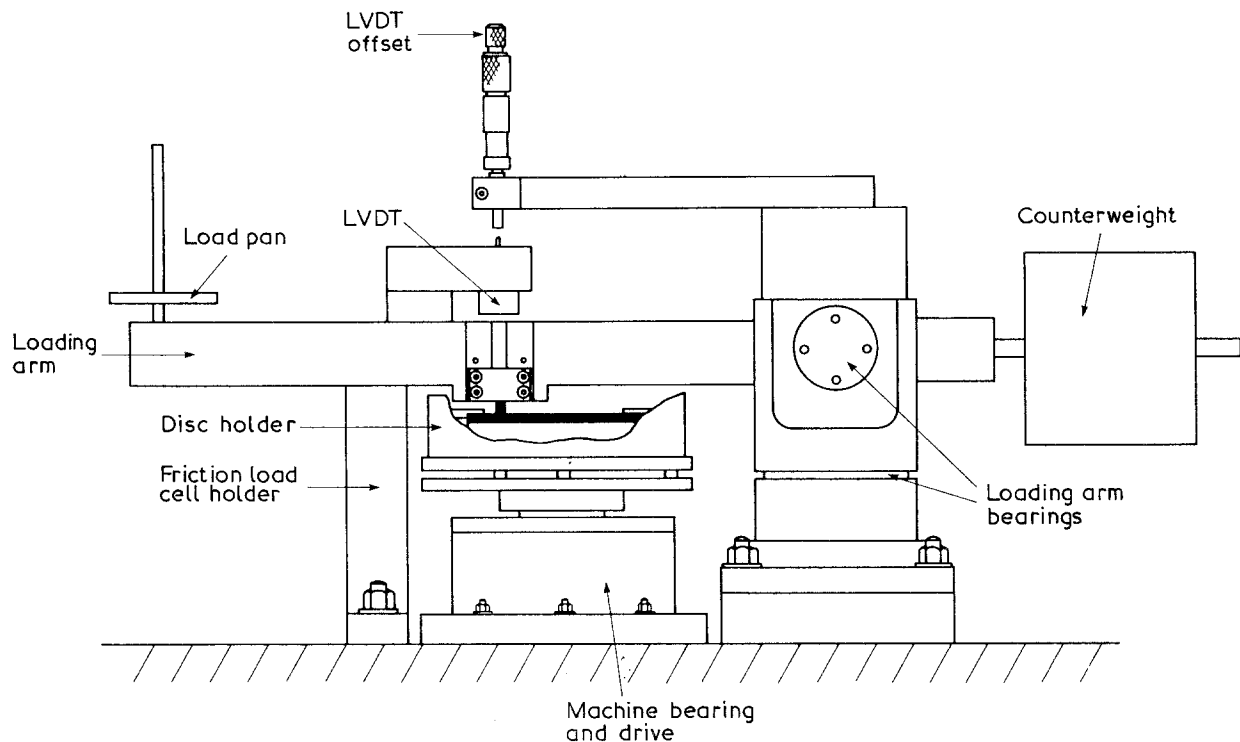


Figure 1 Layout of wear apparatus.

clamped into the loading arm bearing was adjusted to give a wear track diameter of 78 mm and a relative speed of 0.3 m sec^{-1} when the disc was rotated at $0.82 \text{ rev sec}^{-1}$ by the 2.24 kW motor through an infinitely variable gearbox and a belt drive. The rotational speed was checked before and during each test by a hand-held optical tachometer.

Specimens were cleaned before and after testing by immersion in trichlorotrifluoroethane, swabbing with cotton buds soaked in trichlorotrifluoroethane, and drying with paper towels. They were weighed with a microbalance and their profiles measured with a planimeter. The test was started with the pin resting on the surface of the disc, and after an appropriate amount of wear had been detected with the displacement transducer, the specimens were removed, cleaned, reweighed, and their profiles measured.

The temperature and humidity of the test surroundings were not controlled. Measurements taken near the disc-pin interface at the start of the tests showed the temperature varied from 22 to 27°C and the relative humidity varied from 20 to 58%. During the tests the temperature rose by 4 to 6°C and the relative humidity fell by between 3 and 10% of its initial value.

Specimens were examined both before and after testing by optical microscopy, scanning electron microscopy, and some by 850 MHz scanning acoustic microscopy. Measurements of surface roughness were made with a diamond stylus profilometer with a $10 \mu\text{m}$ diameter radius. The instrument provided roughness measurements expressed in terms of Ra values which are equivalent to CLA values.

X-ray diffraction analyses of the pin wear surfaces and wear debris were performed using a counter diffractometer with 20 step widths of 0.02° to 0.04° and count times of 5 to 40 sec at each step. $\text{CrK}\alpha$ radiation was used to minimise penetration of X-rays into the subsurface layers. The Warren and Averbach (WA) and integral breadth (IB) analyses [1, 2] were used to estimate crystallite size and strain for the 012 and 024 alumina peaks (see Appendix).

3. Results

3.1. Wear and friction

Examples of the displacement and friction recordings are shown in Figs 2 to 4, and the results are summarized in Table I together with mass loss measurements. By inspection of the recorder traces it was

TABLE I Wear test results

Test*	Duration (ksec)	Mass change (mg)		Spec. wear rate ($\mu\text{m}^3/\text{N}^{-1} \text{m}^{-1}$)		Friction coefficient		Displacement μm
		pin	disc	pin	disc	start	end	
A10	570	-0.8	-4.7	1300	7600	0.20	0.70	21
A40	251	-0.1	-0.2	-	184	0.25	0.30	0
B10	570	-0.1	-6.3	-	10000	0.70	0.50	8.3
B30	1.1	-2.5	-20.1	52000	420000	0.25	1.25	32
B50	1.6	-6.7	-33.5	77000	390000	0.50	1.05	62
C20	810	-0.1	-6.2	-	350	0.50	0.50	33.1**
C40	1.4	-5.3	-33.3	85000	540000	0.50	0.95	76

*number denotes load in newtons; letter denotes surface preparation.

**for first 0.57 msec of test.

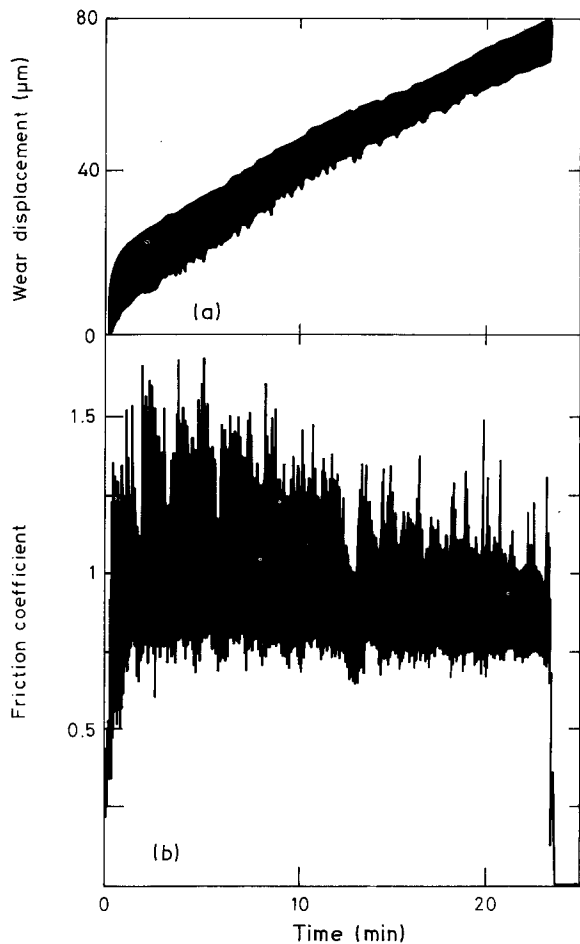


Figure 2 (a) Wear and (b) friction traces for test C40.

possible to discern fluctuations in displacement and friction at two frequencies. Firstly, there was always a fluctuation with a period identical to that of the rotation of the disc. This was probably caused by a residual misalignment of the disc and accounts for the background spread of the traces. Superimposed on the trace, there were abrupt fluctuations of lower frequency, which were of small amplitude in the displacement traces but proportionately larger in the friction traces, especially in tests where the wear rates were high (Fig. 2). In results reported elsewhere [3] it was found that when the test equipment was used on a

99.5% alumina, an additional high frequency fluctuation of about 500 Hz was generated in displacement, load and friction, however these effects were not investigated in the present work.

The results of the measurements of mass losses and displacements are given in Table I, together with calculated values of the specific wear rate which is expressed in dimensions of mass loss per unit load per unit distance. It can be seen that the mass lost by the disc was always greater than that by the pin. At low loads, little wear was observed in any test. For test A10 on lapped and polished specimens, most of the wear (accounting for 16 µm of LVDT displacement) occurred in the initial few minutes of the test. This was due to misalignment of the pin so that all the load was carried initially by a small portion of the pin surface.

At an applied load of 40 N, a clear difference was observed for specimens with different surface finishes. Little wear was observed for the lapped and polished finish (preparation A). However, for ground finish B there was a sharp increase in the wear rate after 150 m of sliding, and at 50 N (B50) the wear rate increased gradually over the first 40 m of sliding and then remained relatively constant for the remainder of the test (Fig. 3). For ground finish C, the wear rate was high for the duration of the test. For both ground finishes, the noise generated during the test became considerably louder when the high wear rates prevailed.

There was considerable variation in the friction coefficients (frictional resistance divided by nominal applied load), both within individual tests, and from test to test (Table I). Generally the friction coefficients were often lower (between 0.2 and 0.5) for tests or parts of tests where the wear rate was low. At high wear rates the friction coefficient was between 0.5 and 1.25 for most of the duration of the test. The sharp increases in wear rates in some tests (B40 and B50) were accompanied by increases in friction (Fig. 3).

3.2. Profiles

The surface roughness measurements expressed as R_a , roughness average, values in Tables II and III were made in the T_g and P_g directions (transverse and

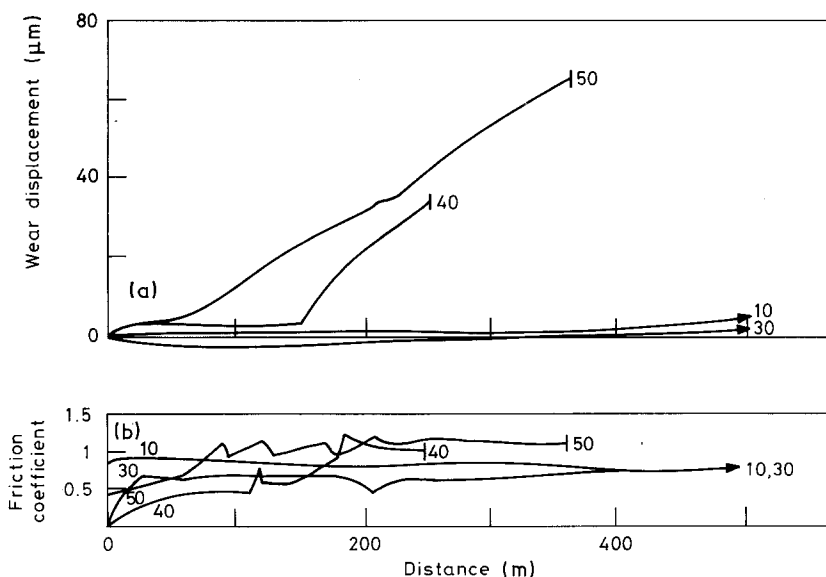


Figure 3 (a) Wear and (b) friction traces for tests B10, B30, B40 and B50.

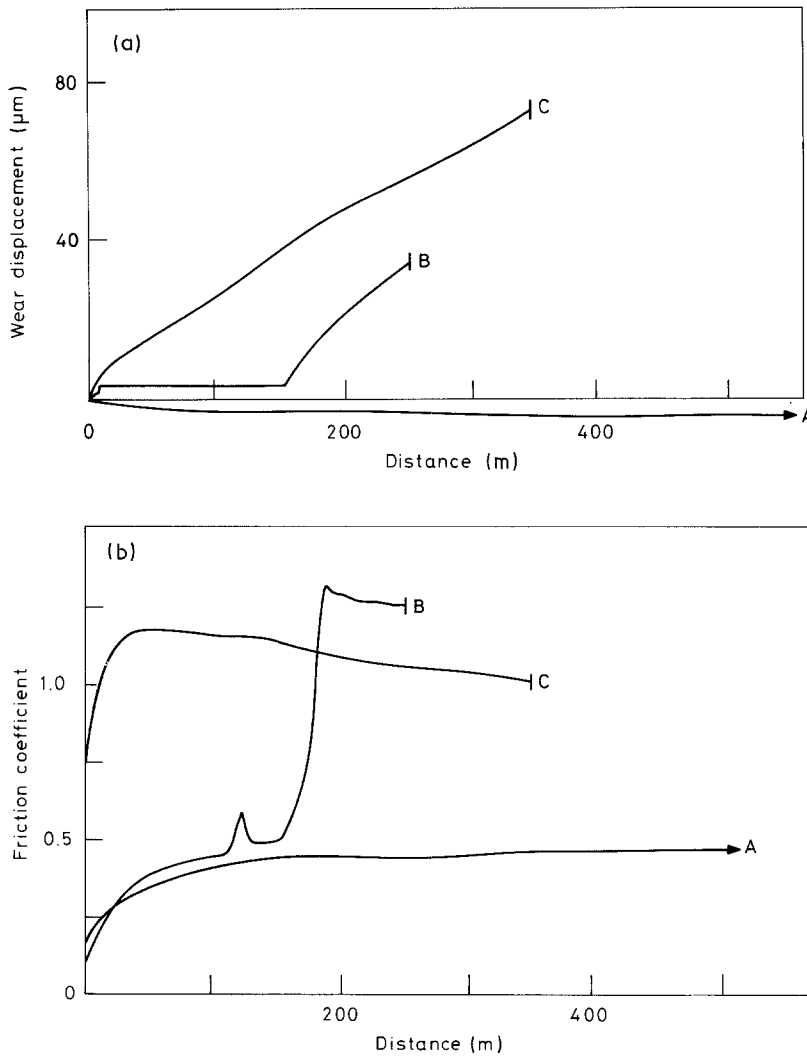


Figure 4 (a) Wear and (b) friction traces for specimens prepared with finishes A, B and C and tested under a 40 N load.

parallel to the grinding directions respectively), and the T_w and P_w directions (transverse and parallel to the wear track respectively) before and after testing.

The initial R_a values of 0.07 to 0.12 μm for the lapped and polished discs were not changed significantly in the T_w nor P_w directions by the wear tests, but the pin surfaces exhibited some roughening.

The two ground finishes B and C, had similar R_a value ranges of about 0.3 to 0.5 μm in the T_g direction, and about 0.2 to 0.45 μm in the P_g direction. However, visual examination showed that for discs with finish B, in addition to the local roughness, there was a periodic variation in flatness with a wavelength of 3 mm.

After wear testing, there was a reduction in the lower range limit in R_a for discs tested at low loads for finish B. More generally however, in the other tests on finishes B and C, there was little change in the R_a value range for the T_g direction, but there was an increase in the P_g direction. The R_a value ranges for the pin surfaces before and after testing showed similar trends to those recorded for the disc surfaces (Table III) but there may have been some anomalies due to the practical problem of setting up the measuring device for small areas.

Examination of the profilometer traces using an expanded distance scale (Figs 5 to 7) for measure-

TABLE II Roughness of discs in μm , before and after testing

Test	Before		After		
	T_g^*	P_g	$T_g T_w$	$P_g T_w$	P_w
A10		0.07-0.12**	0.04-0.20**	-	0.06-0.33
A40		0.08-0.12**	0.07-0.14**	-	0.09-0.13
B10	0.33-0.47		-	0.11-0.28	-
B30	0.36-0.61	0.22-0.44	0.08-0.42	0.12-0.50	-
B40	0.38-0.47	0.26-0.52	0.40-0.80	0.34-0.66	-
B50	0.29-0.47	0.23-0.35	0.22-0.60	0.34-0.60	-
C20	0.27-0.43	0.24-0.38	0.17-0.48	0.29-0.48	-
C40	0.36-0.52	0.17-0.48	0.21-0.67	0.31-0.56	-

* T_g and P_g represent surface roughness measurements made transverse and parallel to the grinding direction respectively before testing; T_w and P_w represent measurements made transverse and parallel to the wear track respectively after testing.

**Lapped surfaces contained no grinding marks.

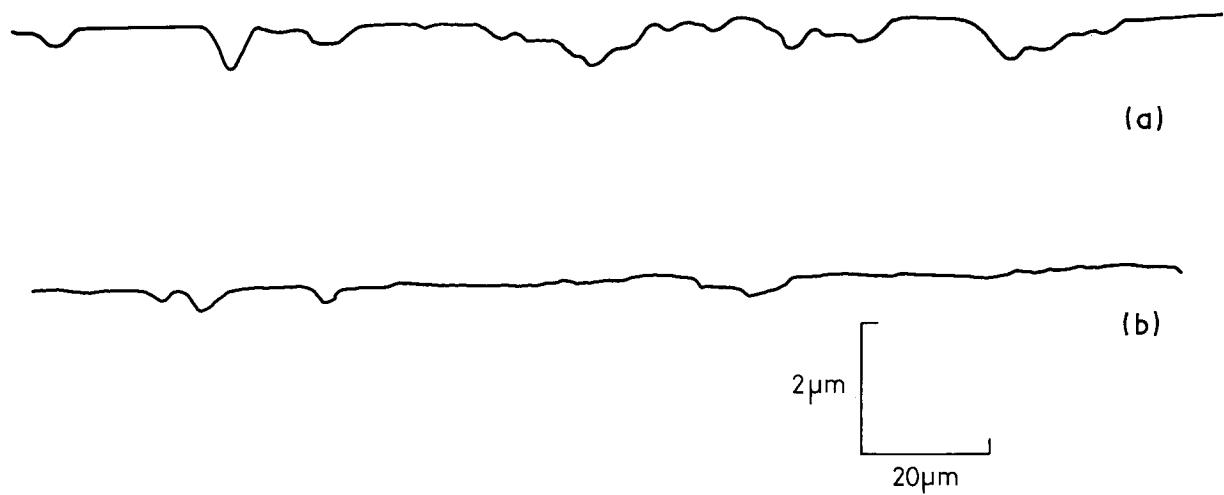


Figure 5 Profiles of lapped and polished discs; (a) before testing, and (b) transverse to wear track direction in test A40.

ments in the T_w direction on discs provided clearer information about the differences in the initial and worn surfaces than could be obtained from the R_a values. The traces for the lapped and polished discs (Fig. 5) were similar before and after testing, and both contained depressions which could be attributed to porosity and "pull-out" (a loss of individual grains or regions of a second phase which is difficult to avoid during surface preparation of brittle materials).

Examination of expanded profiles of the ground surfaces measured in the T_g direction (Figs 6 and 7) shows that surface preparation C gave a distinctly more jagged and irregular profile than was obtained with preparation B. After testing at low loads, the surfaces were unchanged (B30) or became smoother (B30 and C20), but testing at higher loads increased the amplitude and wavelength of the fluctuations in the profiles to a similar extent for finishes B and C.

3.3. Microscopy

Micrographs of the surface finishes produced by preparations A and B are shown in Figs 8a and b together with taper sections (Figs 8c and d) which show that grinding produced subsurface cracks, but lapping and polishing did not visibly affect the subsurface layers. The wear tracks on discs with preparation A could only be identified by a slight change in contrast between the wear track and undamaged surface (Fig. 9a). However, wear tracks on discs with ground

finishes were clearly visible, and there were clear differences in appearance of wear tracks transverse and parallel to the grinding direction (Figs 9b and c). The surface of pins used in tests where little wear took place, showed wear at only one side of the pin. In tests where high wear had occurred, the entire surface was worn.

Examination of the wear surface on disc A40 showed that scratches and apparent porosity in the original lapped surface (Fig. 8d), had been removed, and some of the alumina grains were depressed relative to others (Fig. 10).

A prominent feature of the worn areas on specimens with ground finishes B and C was the high incidence of networks of cracks which extended over quite large areas (Fig. 11a). There were a considerable number in the highly worn material but fewer in the lightly worn. They were equally prevalent when the wear track ran perpendicular or parallel to the grinding direction. Scanning acoustic microscopy confirmed the presence of the crack networks (Fig. 11b).

Nomarski optical interference microscopy showed that there were fine grooves, typically 40 to 60 μm long (Fig. 12a), over most of the worn areas of the ground surfaces. Another feature was regions of buckling and elevation of the surface relative to the surroundings. These areas were always bounded by cracks.

3.4. X-ray diffraction

Examples of traces obtained from the powders and pin surfaces are compared with a trace obtained from strain-free 50 μm alumina grit in Fig. 13. There was considerable broadening of the peaks for the powders but very little for the pin surfaces.

The strain and particle size measurements obtained from the WA and IB analyses are given in Table IV. Because of uncertainties in the WA estimates of strain (see Appendix) it is not possible to give a single value. Instead the spread in values of the root mean square strain at 10 and 15 nm are taken as representative. Some measurements were also performed on powder debris from earlier tests on alumina [4].

The plot of β^{*2} against d^{*2} shown in Fig. 14 was used to determine size and strain in the IB method (β^* in the peak integral breadth corrected for instrumental

TABLE III Roughness of pins in μm , before and after testing

Test	Before		After	
	T_g^*	P_g	T_w	P_w
A10	0.03–0.07	–	0.12–0.36	0.03–0.70
A40	–	–	0.03–0.18	0.11–0.56
B10	–	–	0.29–0.55	0.03–0.18
B30	0.36–0.56	0.20–0.37	0.03	–
B40	–	–	0.24–0.46	0.05–0.24
B50	–	–	0.37–0.60	0.30–0.49
C20	–	–	0.13–0.38	0.18–0.29
C40	0.26–0.37	0.21–0.33	0.33–0.70	0.34–0.63

* T_g and P_g represent surface roughness measurements made transverse and parallel to the grinding direction respectively before testing; T_w and P_w represent measurements made transverse and parallel to the wear track respectively after testing.

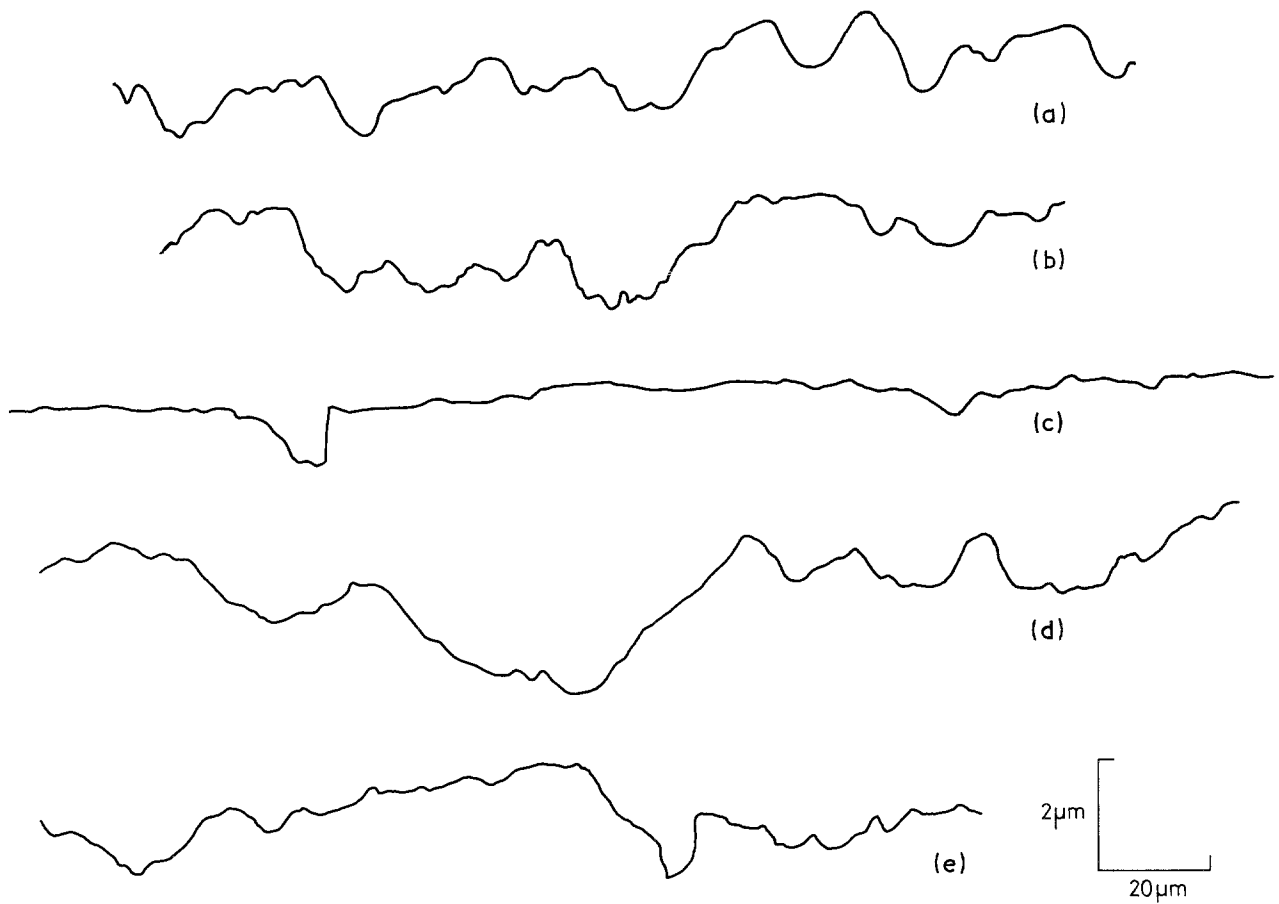


Figure 6 Profiles transverse to grinding and wear track directions for surface preparation B; (a) before testing, (b) tests B10, (c) test B30, (d) test B40, and (e) test B50.

effects and d^* is the reciprocal distance $2\sin \theta/\lambda$). The strain was determined from the slope of β^{*2} against d^{*2} , but the plots show considerable deviations from linearity. This was mainly due to an anisotropy in particle dimensions relative to crystal orientation, which restricted the size and strain determinations to 012 and 024, the only multiple reflections available. There was also some uncertainty in the β^{*2} values because relative to the level of the background noise, the count rate was low for the small amounts of debris available (Fig. 13).

For the powder debris, the WA effective size L_c was

about 10 to 20 nm and the IB effective size L_s was about 20 to 40 nm. This small difference was expected and was in good agreement with the theories since they derived different statistical parameters for the particle size (see Appendix). There was also a possible contribution from twinning or stacking faults which could not be determined by the methods. However, the X-ray size measurements were in qualitative agreement with electron microscopy observations which showed aggregates of particles of different orientations and with diameters of about 20 nm.

The WA root mean square strain $\langle \Sigma^2 \rangle^{1/2}$ for the

TABLE IV X-ray line broadening results

Wear debris test	Warren-Averbach method			Integral breadth method	
	Size (nm)	Strain $\times 10^3$		Size (nm)	Strain $\times 10^3$
		$L = 10$ nm	$L = 15$ nm		
A40	–	–	–	34	9
B40	15	3.2	1.8–2.7	40	5
B50	17	4.0	2.4–3.3	23	6
C40	16	3.2–3.6	1.5–2.2	–	4
A/A/27*	12	1.7–2.4	1.4–2.3	30	8
A/A/73	14	1.2–2.6	2.2–2.7	–	–
A/A/74	12	1.6–2.4	1.7–2.4	–	–
Pin surface					
A10	104	0	0	–	1.0
B10	89	0	0	150	0.7
B30	69	0	0	133	0.6
B40	64	0	0	114	0.8
B50	57	0	0	85	1.0
C20	–	–	–	124	0.6
C40	55	0	0	130	1.0

*Wear debris from tests reported elsewhere, [3].

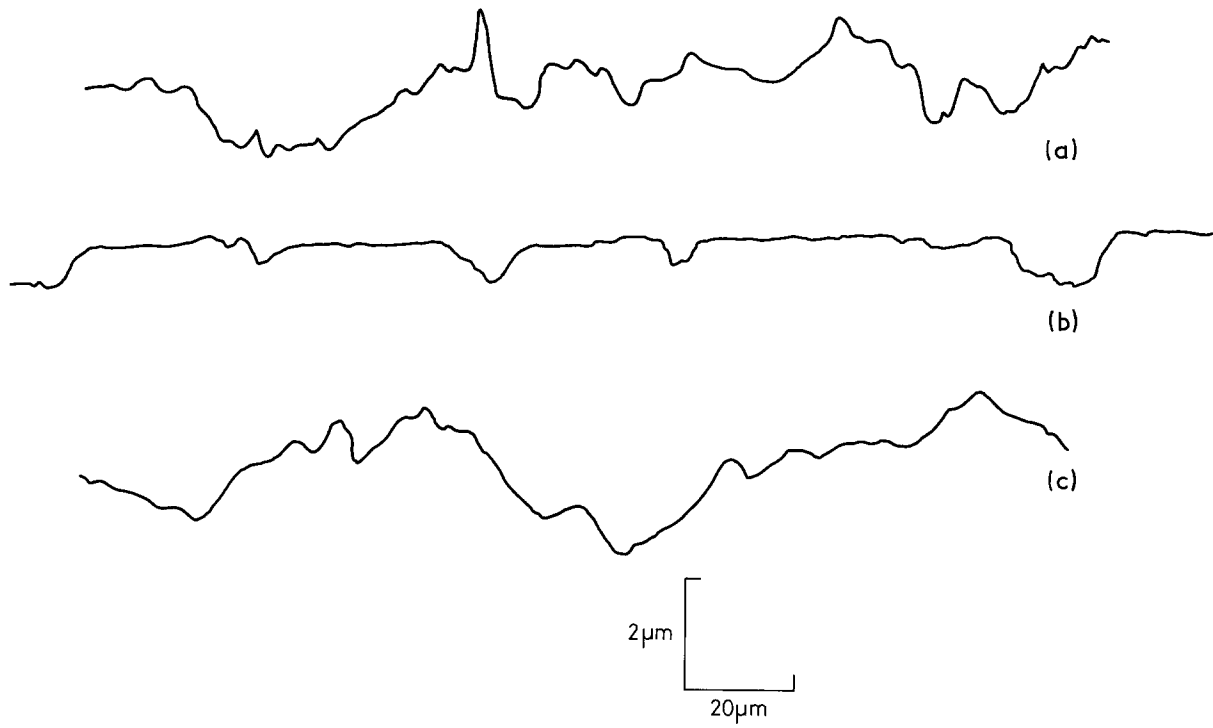


Figure 7 Profiles transverse to grinding and wear track directions for surface preparation C; (a) before testing, (b) test C20, and (c) test C40.

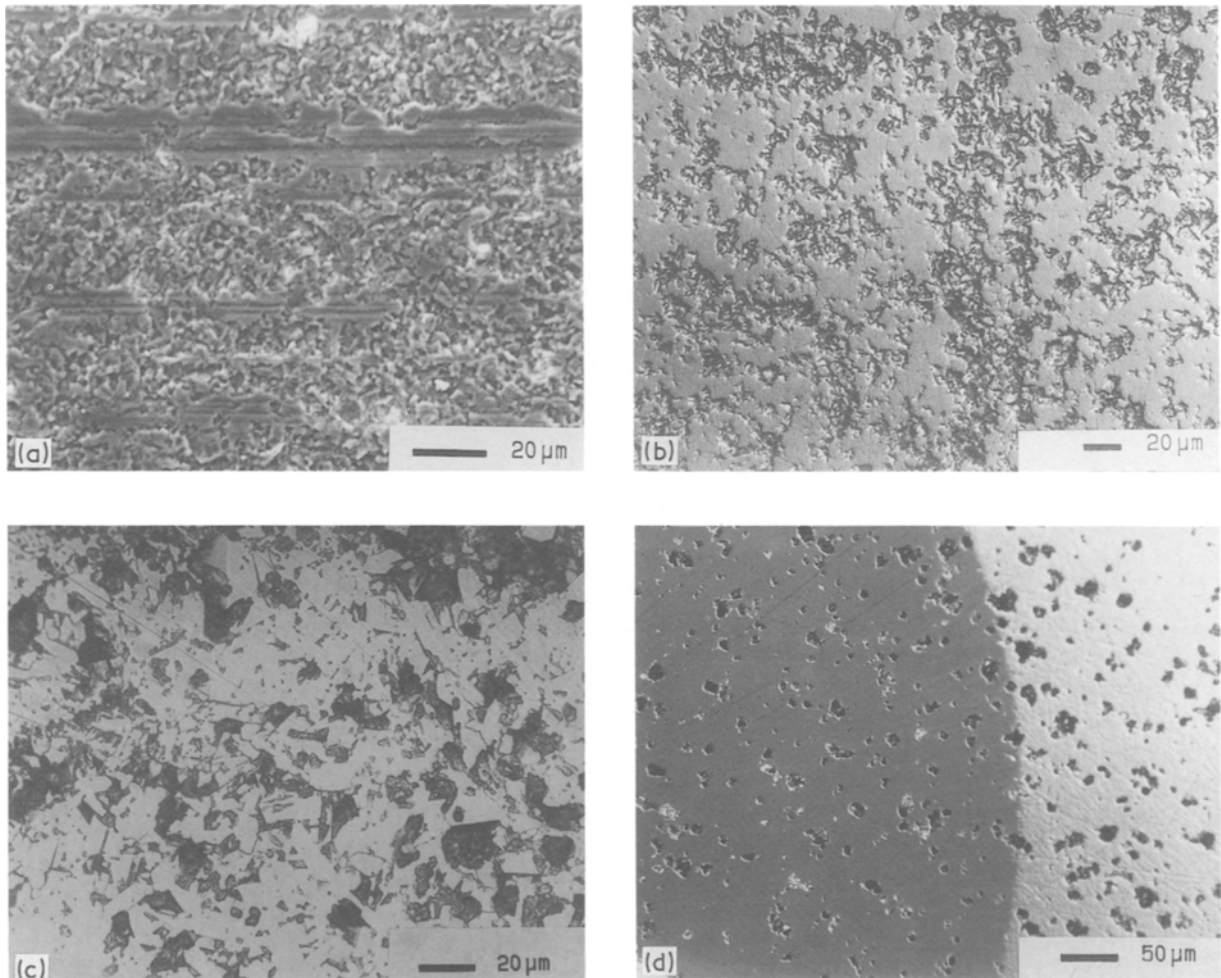


Figure 8 (a) Scanning electron micrograph of ground finish, (b) No marski optical interference micrograph of lapped and polished finish (c) tapered section formed by cratering of ground surface, and (d) edge of crater formed on lapped and polished surface.

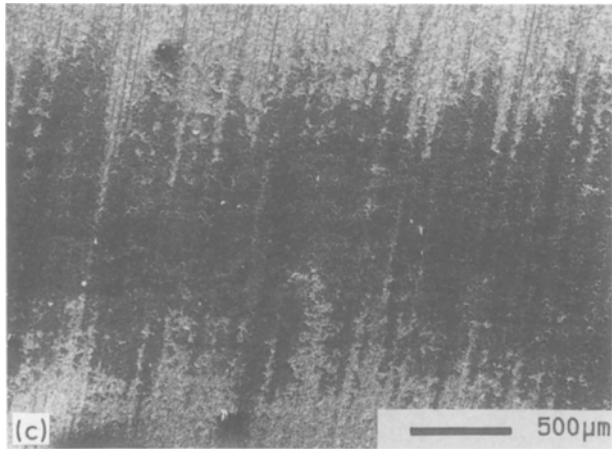
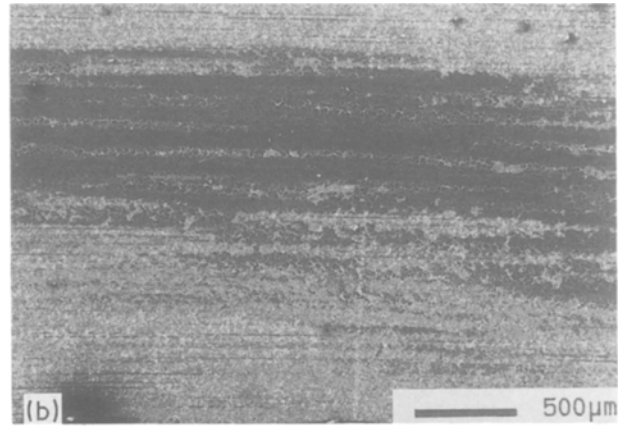
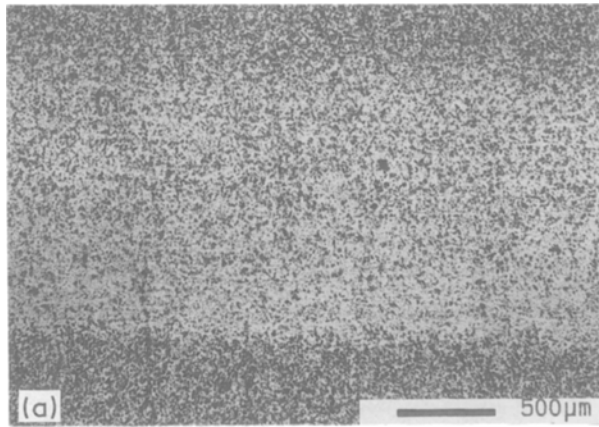


Figure 9 (a) Optical micrograph of wear track formed on disc A40, (b) scanning electron micrograph of wear track formed parallel to grinding direction on disc B10, and (c) scanning electron micrograph of wear track formed transverse to grinding direction on disc B10.

debris varied between 0.012 and 0.040 for an L of 10 nm and 0.014 and 0.033 for an L of 15 nm. This compares with the values obtained for the IB strain e of 0.04 and 0.09. There was no obvious reason for the disagreement in the two results since according to the theoretical relationship

$$e = 1.25 \langle \Sigma^2 \rangle^{1/2}$$

The strain in the pin surfaces was found to be between 0.0006 and 0.001 by the IB method, but was undetectable by the WA method. However, at such small values the IB technique is thought to be unreliable because assumptions in the analysis become invalid, and the values measured for the count rate are comparable in magnitude with the background noise in the equipment.

For the pin surfaces the effective size L_c measured by the WA method varied between 55 and 104 nm. These sizes were much smaller than the alumina grain size which was about 5 μm, and consequently there is some evidence that the surface grains may have broken up into crystallites or fragments. Unfortunately it was not possible to get convincing evidence of this possibility since because of experimental limitations it was difficult to obtain accurate estimates of particle sizes greater than 100 nm due to the decrease in the line broadening beyond this value.

The depth of penetration of the X-rays determines the volume of material sampled, such that if the fraction of X-rays that is absorbed by a surface is F , where

[5]

$$F = \exp\left(\frac{-2\mu z}{\sin \theta}\right)$$

where μ is the mass absorption coefficient for the material, z the depth, and θ the diffraction angle. For CrK_α radiation and alumina, 90% of the X-rays were absorbed at depths of 12 and 24 μm at 20 angles of 38.4 for 0.12 reflections and 82.4 for 0.24 reflections respectively. At depths between 4 and 7 μm, 50% of the X-rays were absorbed. These depths were comparable to or larger than the grain size, so that if plastic strain only occurs in the uppermost layers of the surface grains, the averaged strain in the sampled volume would be low and the line broadening would be correspondingly small.

The values obtained for the effective particle sizes and strains were similar to those found in other investigations (Table V). For example, Cutter and McPherson [6] obtained a particle size of 30 nm and a WA strain of 0.0003, and an IB strain of 0.0019 for wear debris detached in sliding tests on alumina specimens submerged in alcohol. Similarly, Lewis and Wheeler [7] measured a particle size of 20 to 30 nm and an IB strain of 0.067 for alumina specimens that had been vibratory milled.

4. Discussion

Important practical and scientific implications arise from the observation of the low specific wear rate for the lapped and polished surfaces at a 40 N applied load compared with the 10 to 100 fold increase in the same parameter for the ground surfaces at loads of 40 N. For clearly it would help industry to assess the viability of alumina for specific wear applications if a mechanistic explanation could be provided which helped to define the best combination of surface finish, materials characteristics and service conditions to ensure that the component always operated in a low wear regime.

An essential component of models for sliding wear of brittle materials is the removal of asperities from

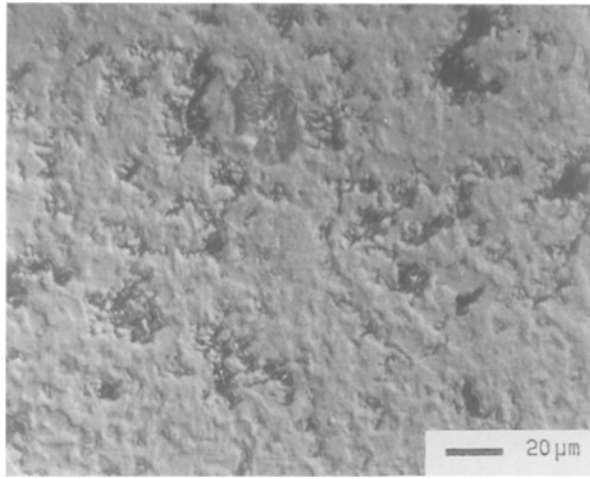


Figure 10 No marski optical interference micrograph of wear surface of disc A40.

the wear counterfaces and the subsequent involvement of the detached material in the wear process. It may, for example, after breaking away, serve an active role by behaving as micro-indenters as in abrasive wear mechanisms; however, for the applied loads and sizes of particles involved in the present work, the size of

indentation would be far too small to produce micro-cracking. Consequently if the wear debris did participate in a mechanism for material removal, it probably contributed more in the low wear regime than in the high wear regime which was characterized by a high incidence of surface cracking.

Because of the association of heavy surface cracking with the high wear rates, a satisfactory explanation must provide for a self sustaining mechanism for crack generation. The simplest explanation would be that the underlying material is damaged when an asperity breaks away from the surface. A second possibility is that the sliding action generates sufficient heat to cause thermal cracking during the cyclic heating and cooling that occurs in individual regions of the wear track as they come into periodic contact with the pin during each revolution. A third possibility, is that indentation cracks are produced at points of contact with asperities on the counterface surface but this appears to be unlikely for the same reasoning as was given for the debris performing such a role. The explanation which appears to fit the current results and those obtained elsewhere most satisfactorily, is one involving a mechanism whereby subsurface cracks grow in a regular mosaic pattern until regions of the surface are so weakened that flakes can be detached by

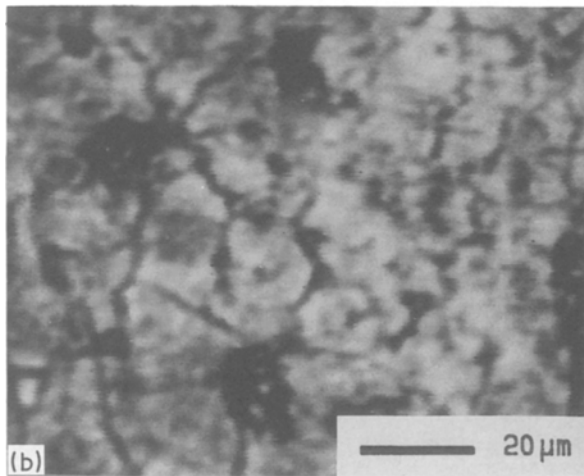
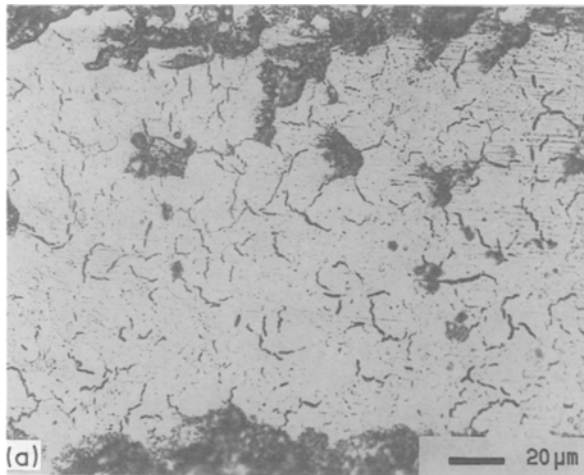


Figure 11 (a) Optical micrograph of wear track on alumina disc C20 parallel to grinding direction, and (b) scanning acoustic micrograph of wear track on disc B10.

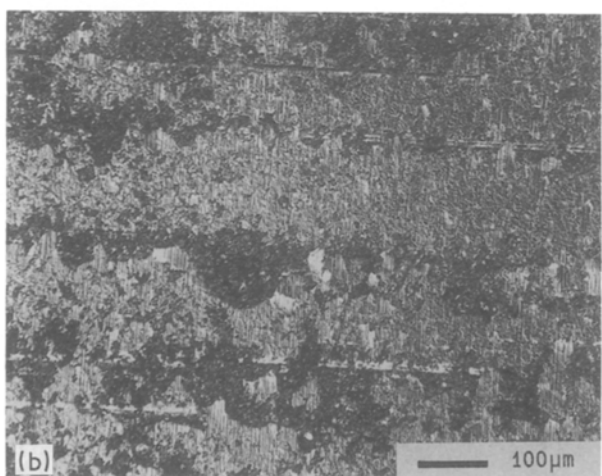
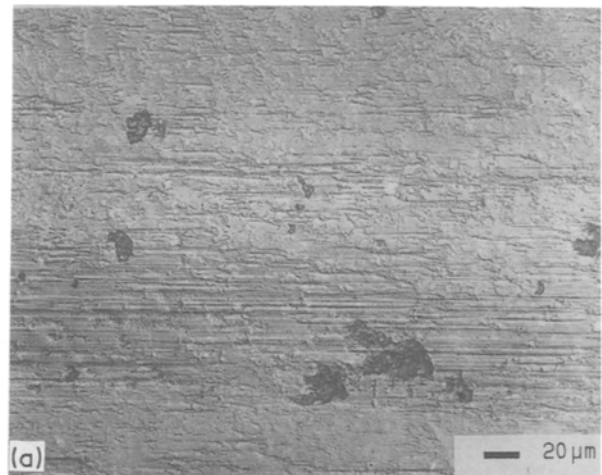


Figure 12 No marski optical interference micrographs of wear track on disc B10, (a) transverse to grinding direction, and (b) parallel to grinding direction.

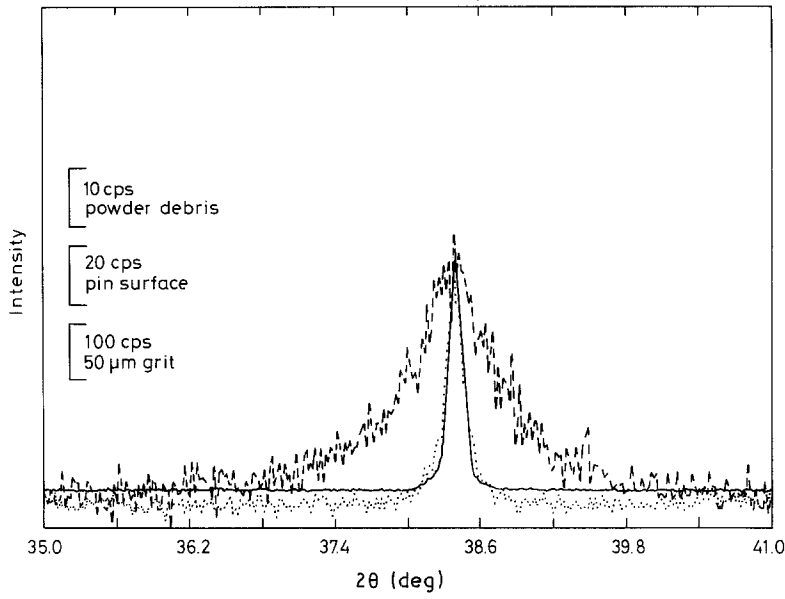


Figure 13 Typical X-ray diffraction traces in cps (counts per second) obtained from the wear debris (----) the pin surface (····) and a strain-free 50 μm grit (—).

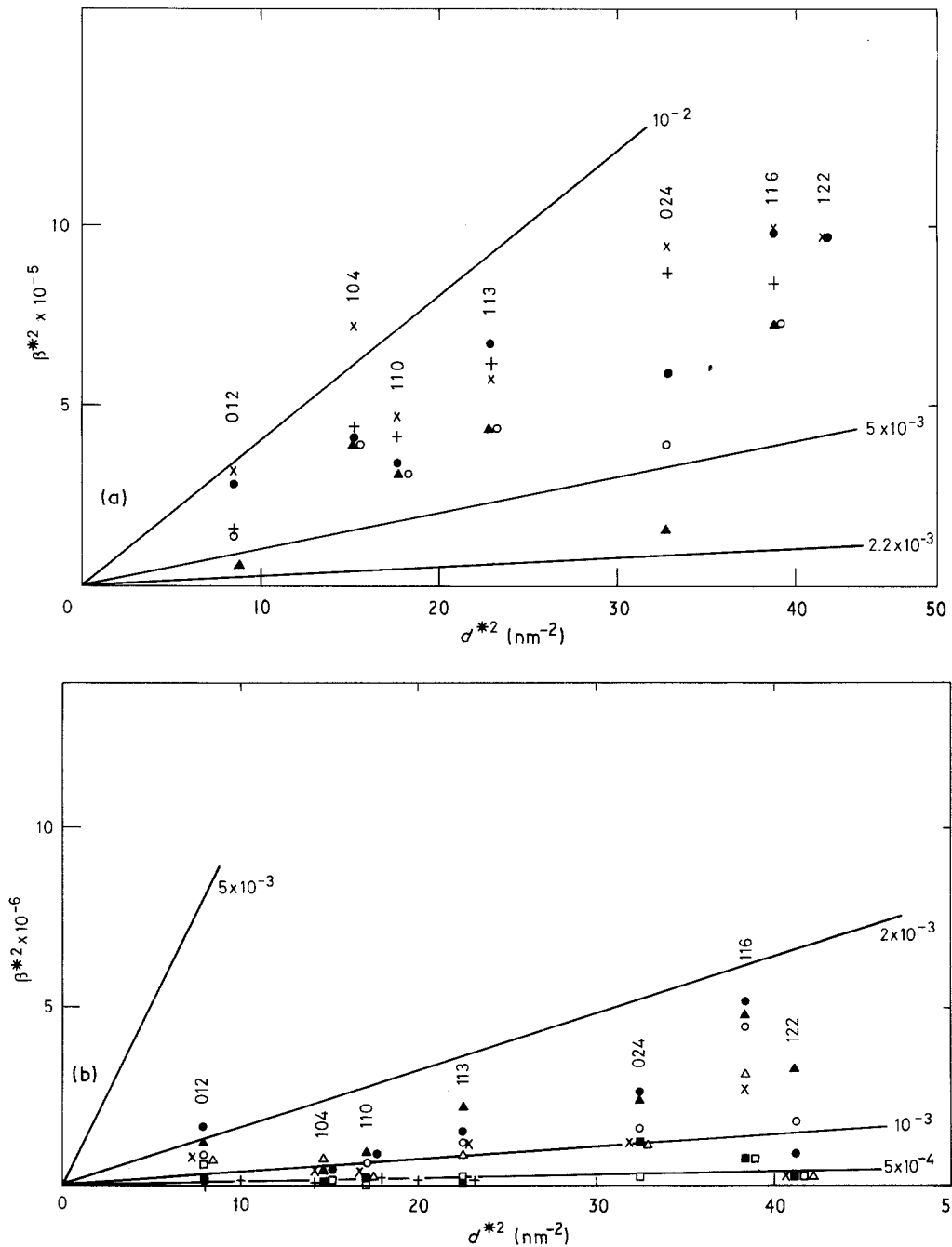


Figure 14 Plots of β^{*2} against d^{*2} for (a) wear debris, and (b) pin surfaces (\times A/A/27, \bullet B50, \circ B40, $+$ A40, \blacktriangle C40) (\blacksquare A10, $+$ A40, \square B10, \triangle B30, \circ B40, \bullet B50, \times C20, \blacktriangle C40).

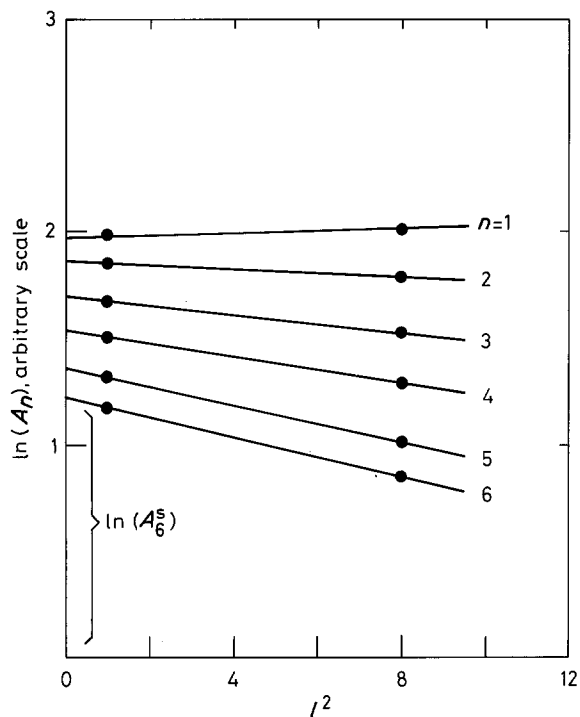


Figure 15 Typical plots of $\ln(A_n)$ against l^2 . The root mean square strain $\langle \Sigma^2 \rangle^{1/2}$ can be derived from the slopes of the lines $2(\pi n)^2 \times \langle \Sigma^2 \rangle$, and the size coefficients A_n^s are given by the $l^2 = 0$ intercepts.

impact with a protrusion on the counterface surface. In order to consider the contribution of this mechanism to the high wear rates and to discuss the processes involved in the low wear regime it is helpful to examine existing knowledge of deformation mechanisms in alumina in more detail in relation to the present results.

4.1. Low wear regime

Characteristic features of the low wear regime were that: the conditions favoured neither the initiation nor propagation of microcracks; the lapped and polished surfaces became smoother as a result of the elimination of apparent porosity and coarse scratches; a surface relief effect was produced whereby some grains

were depressed relative to their neighbours; the asperities were removed from the ground surfaces. In the absence of microcracking as a major vehicle for material removal it is necessary to examine the possibilities of a contribution from plastic deformation.

The currently accepted view on plasticity in alumina [8–10] is that up to 1650°C slip is confined to the basal and prismatic planes, which provide only four independent systems. Under certain conditions, such as hydrostatic compression and possibly beneath pyramid indenters, the occurrence of glide on pyramidal planes enables the general deformation tensor for five systems to be satisfied at temperatures as low as 1150°C. However, normally brittle fracture occurs below 1100°C, while grain boundary sliding occurs above that temperature, and the role of twinning is still unknown. As a result, the conditions for plastic deformation in alumina are still poorly understood. Nevertheless, because of the restriction on slip, it is well established that grain boundary cracking is needed to accommodate non-elastic displacements. Even when general plasticity is possible, cracking may occur in preference to plasticity because of the high resolved shear stresses required to move dislocations.

The results from the X-ray diffraction analyses of worn pin surfaces indicate that if plastic deformation occurred it would have been very limited in extent. Combining this fact with the theoretical restrictions on slip, it appears that plastic deformation could have occurred provided it was confined to a surface layer of depth less than one grain diameter where the conditions for general slip would be relaxed. This possibility would be compatible with an explanation for the surface relief effects involving preferential wear of grains with orientations of lowest resistance to plastic deformation such as would be expected for basal planes parallel to the surface in alumina [11, 12]. However, for this explanation to be acceptable, it is still necessary to postulate a mechanism for removing the surface material. One possibility would be that the surfaces are abraded by fine wear debris and material is regularly detached to replenish the supply of

TABLE V Literature values for particle size and strain by X-ray line broadening and TEM measurements

Material	Method	Particle size (nm)	Strain $\times 10^3$	Reference
Magnesia abraded in alcohol	IB	29, 37, 55	1.0–1.5	[15]
Magnesia abraded in alcohol	IB	30	4	[16]
Alumina abraded in alcohol	WA	30	3	[17]
Alumina abraded in alcohol	IB	30	1.9	[6]
Alumina, vibratory milled	IB	20–30	6.7	[6]
Titania abraded in air	TEM*	10	–	[17]
Various ceramics	TEM	< 10	–	[18]
Silicon carbide wear test	TEM	5–20	–	[19]
Partly stabilised zirconia, wear test	TEM	5–50	–	[19]

TEM* – Transmission electron microscope, direct measurement from images.

abrasive particles. Unfortunately the amount of wear debris was insufficient in the low wear regime to make realistic measurements of the particle size. However, the generation of 10 to 30 nm particles in the high wear regime, and the observation of fine grooving on all wear surfaces (Fig. 12) indicates that fine scale abrasion may have occurred in all tests but made a negligible contribution to the higher wear rates. Under the latter conditions, the source of fine abrasive particles from incremental wear of asperities or from comminution of detached asperities would be more profuse and the grooving more widespread.

4.2. High wear regime

Characteristic features of the high wear regime were: it occurred in tests on the ground surfaces at an applied load of 40 N but did not occur in tests on the lapped and polished surfaces; it did not operate immediately in tests on specimens with preparation B, but required an incubation period of wear; it was accompanied by a high incidence of surface cracking.

Concentration on processes involving subsurface crack growth whilst not eliminating a possible contribution from indentation or thermal cracking, it is adequate to explore their ability to explain the results without providing a detailed mechanism of their operation. Nevertheless it is helpful to define some essentials of a suitable mechanism. In one model, the pre-existing subsurface cracks burrow ahead of the surface layer by fatigue crack growth under cyclic loading, and periodically undermine regions of the surface structure so much that they can be easily detached by impact by protuberances on the counterface surface. According to this model [3], the high wear resistance of the lapped and polished surfaces, can be attributed to the initial absence of surface and subsurface cracks which means that the process for weakening the surface layers cannot be initiated. The need to exceed a critical load to achieve high wear rates in specimens with ground surfaces is consistent with the existence of threshold values for the loads needed to achieve significant fatigue crack growth. Yust and Carignan have also proposed a contribution from fatigue crack growth in the wear of ceramics [13]. Other support for the proposed explanation is found in the work of Enomoto *et al.* who observed that wear rates and friction increase with increase in initial surface roughness in sliding wear tests on alumina, and that subsurface microcracks were present at high wear rates [14]. The observation of an incubation period of slow wear prior to the onset of fast wear for preparation B, implies that the surface layers underwent an initial conditioning process, possibly involving some modification of the initial profile before the subsurface crack propagation mechanism could operate effectively. Thus preparation B gave a surface which was initially smoother and contained less stress concentrations for promoting crack growth and propagation; also smoother surfaces at the wear interface would decrease the amount of self induced vibration which assist fatigue crack growth. Severe wear probably started when the surface and subsurface cracks had undermined the initial surface sufficiently to cause

roughening to the same extent at that observed for surfaces with preparation C. This explanation is supported by the observation that the worn surfaces of discs prepared by methods B and C had similar profiles even though they were initially different. It indicates that when a steady state of high wear is established, a characteristic wear profile and surface damage zone are also established for each combination of wear variables irrespective of the initial surface condition.

The occurrence of the surface incubation period is probably related to the use of different grinding wheels in the surface preparations. Thus the use of a resin bonded wheel for treatments A and B would result in the transfer of a light coating of the resin to provide a low friction surface until it was worn away. The use of a metallic bonded wheel for treatment C does not appear to have had any effect.

4.3. Other considerations

Although fatigue crack growth, has been invoked as the mechanism responsible for the high wear rates, other models for subsurface cracking processes, such as shear crack propagation parallel to the surface, could explain most of the results. Also of importance are sources of vibration in the wear system, and environmental fatigue. In alumina the latter will promote growth of cracks in stressed surfaces subjected to humid or aqueous environments, and the wear rate will increase as a result of the deterioration in surface integrity. The effect will probably not be significant at high wear rates but could be serious in the low wear rate regime if coarse abrasive particles become entrapped between the surface and cause surface cracking, or if the alumina contains a grain boundary phase which is susceptible to preferential attack by water.

Vibrations in a wear system come from internal and external sources. For example, the system may experience externally excited vibrations emanating from the motion of the drive motor or nearby machinery. The internally excited vibrations are generated by the fluctuating passage of one counterface over the other and are amplified or reduced by the response of the loading system. Vibrations in a system are known to increase wear rates and an explanation in terms of enhanced fatigue crack growth has been proposed for brittle materials. If, as the present results indicate, there is a threshold load for entering the high wear rate regime, it is likely that vibrations in the system would lower the threshold value by increasing the fatigue crack growth rate and thereby increasing the deterioration of the surface integrity.

Of equal importance is that attention should be paid to ensuring that lapping and polishing treatments remove all subsurface damage since failure to do so, could result in an initial low wear rate altering to a high wear rate once the subsurface cracks have grown sufficiently to undermine the surface, according to the mechanism suggested above for surfaces with preparation B.

5. Conclusions

The results indicate that during dry sliding wear,

alumina can experience low or very high wear rates depending on surface preparation and applied load. Several important implications can be derived from the results and from theoretical explanations for the observations. The most important are that to use alumina successfully under sliding wear conditions, it is necessary:

(i) to lap and polish the surface and to ensure that no residual damage exists below the surface as a result of prior preparations;

(ii) to ensure that all sources of vibration, external and internally generated, are eliminated or minimised;

(iii) to prevent the ingress of abrasive particles into the wear system, and to make conditions unfavourable for environmental fatigue.

It was found that ground surfaces could give an initially low wear rate which increased markedly when the initial surface layer had been worn into a rougher profile, probably by a process of surface and subsurface crack growth.

Theoretical explanations can be made for the existence of low and high wear regimes: low wear rates are attributed to fine scale abrasion by plastic ploughing mechanism; high wear rates are compatible with mechanisms which involve subsurface crack propagation and a consequent undermining of the surface integrity.

X-ray observations on highly worn specimens were compatible with the generation of wear debris of about 20 nm diameter which had been plastically strained by up to 1%: pin wear surfaces contained 5 μm grains which were fragmented into crystallites of 55 to 104 nm thickness: the presence of a plastic strain could not be conclusively established but one method suggested it could be 0.1%.

Appendix

Two techniques were used to estimate the contributions to line broadening from the affects of particle size and stress, and to eliminate instrumental effects. These were the Warren–Averbach (WA) Fourier analysis and integral-breadth (IB) technique. For both methods, peaks from the samples were compared with standard peaks obtained under identical conditions from strain-free particles of alumina powder. An α -alumina lapping compound of 0.25 μm diameter was used for the majority of the WA analyses, and a 5 μm alumina grit was used for one WA analysis and all the IB analyses.

Warren Averbach method

The WA method uses Fourier deconvolution of two orders of peaks diffracted from the same set of lattice planes. For alumina and CrK α radiation the 012 and 024 peaks were the only planes suitable. After deconvolution of the sample and the standard peaks, the corrected Fourier coefficients for the peaks was given by

$$A_n = A_n^s \times A_n^d$$

where n is the order of the coefficient, A_n^s is the contribution due to size broadening, and A_n^d is the contribution due to permanent strain in the material. Theory

shows that

$$A_n^s = N_n/N_\alpha \quad \text{and} \quad A_n^d = \langle \cos 2\pi l Z_n \rangle$$

where N_n is the average number of crystallographic unit cells with neighbours in the same column (a stack of unit cells oriented perpendicular to the diffracting planes), N_α is the average number of cells in a column, l the order of the diffraction peak and Z_n is the difference in distortion displacement of cells that are n unit cells apart. On the assumption that lZ_n is small

$$\langle \cos 2\pi l Z_n \rangle \rightarrow 1 - 2(\pi l)^2 \times \langle Z_n^2 \rangle$$

Also since:

$$\Sigma = Z_n/n$$

and

$$\ln A_n(l) = \ln A_n^s - 2(\pi l n)^2 \times \langle \Sigma^2 \rangle$$

plotting $\ln A_n$ against l^2 gives the size coefficients, A_n^s , at the l^2 equals zero intercepts, and the root mean square value of the strain, can be calculated from the slopes as shown in Fig. 15.

For every coefficient, A_n , a value of strain was calculated. This was the component of strain normal to the diffracting planes averaged over the length $L = na$, after squaring and averaging over all the sample. These strain values are not expected to be reliable at low values of n because of experimental uncertainty in the choice of background level. The strain values also generally decrease with increasing L . This decrease has been attributed to inhomogeneity in strain, and also to a possible fall of contributions with increasing L of the smallest crystallites which probably have the larger strain (Fig. 16).

When the size coefficients A_n^s are plotted against n , the zero intercept for A_n^s is N_α . This gives L_c equals $N_\alpha a$, the average coefficient crystallite dimension perpendicular to the diffraction planes (Fig. 17).

Integral breadth method

In the integral breadth method, the peak integral breadths were determined by dividing the net peak integral by the net peak height. An empirical correction was then set for elimination of instrument broadening effects. In the present analysis, the formula:

$$\beta_c^*/\beta_T^* = 1 - (\beta_I^*/\beta_T^*)^2$$

was used, where β_T^* and β_I^* were the experimentally determined integral breadths for the sample and standard respectively, and β_c^* was the corrected integral breadth. The relation

$$\beta_c^{*2} = 1/L_s^2 + (2ed^*)^2$$

was used to estimate the effective crystallite dimensions L_s , and the strain e by plotting β^{*2} against d^{*2} (Fig. 14). In this relation

$$d^* = 2 \sin \theta / \lambda$$

and the strain e is approximately $\delta d/d_{\text{th}}$. Also e equals $1.25 \langle \Sigma^2 \rangle^{1/2}$. Since the size of the crystallite will vary with crystallographic orientation, the strain e can only be calculated for peaks which are different orders of reflection from the same crystallographic planes, in

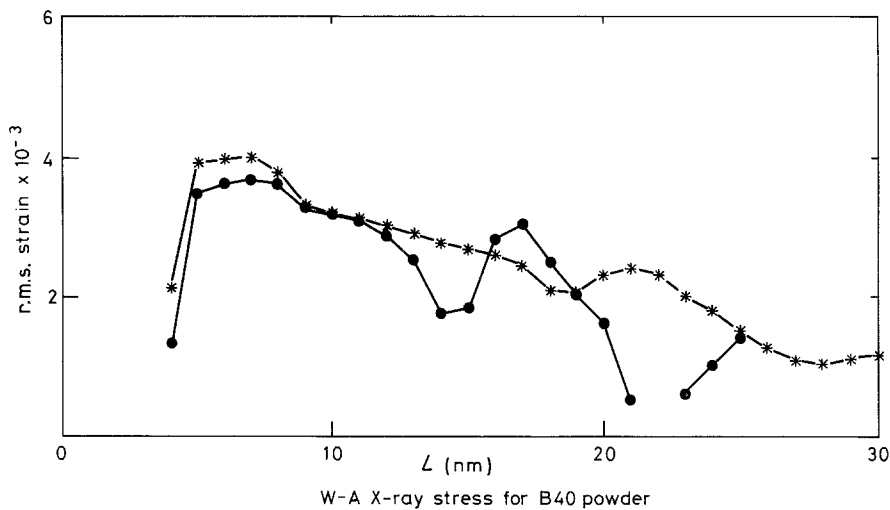


Figure 16 Typical plot of root mean square strain $\langle \Sigma^2 \rangle^{1/2}$ against length parameter L . The two curves are independent measurements.

the present work the 012 planes (i.e. the 012 and 024 peaks of alumina).

Particle size and faulting

Both the true particle size and faulting in the material contribute to line broadening. Thus if L_c and L_s are the effective particle sizes obtained from the WA and IB analyses respectively, the relative contribution of true particle size and faulting is given by

$$1/L_c = 1/L_{cT} + 1/L_{cF}$$

and

$$1/L_s = 1/L_{sT} + 1/L_{sF}$$

where L_{cT} and L_{sT} are the true particle sizes and L_{cF} and L_{sF} are fictitious particle sizes which take account of faulting in the material. However,

$$L_{sF} = 2L_{cF}, \quad L_{sT} = \langle D^2 \rangle / D \quad \text{and} \quad L_{cT} = D$$

where D is an individual crystallite size and $\langle D^2 \rangle / D$ the average crystal size. Thus L_s should theoretically always be larger than L_c because $\langle D^2 \rangle / D > D$ for any spread in particle sizes.

The contribution of the line broadening from faulting can only be separated from the true size contribution by analysis of multiple-order reflections from two or more sets of crystallographic planes; however there is only one set of reflections available for alumina with

CrK α X-radiation, and consequently, an analysis for faulting could not be performed.

References

1. C. N. J. WAGNER, "Local Atomic Arrangements studied by X-Ray Diffraction, Metallurgical Society Conferences 36", (Gordon and Breach, New York, 1966) pp. 219-264.
2. H. P. KLUG and L. E. ALEXANDER, "X-Ray Diffraction Procedures for Polycrystalline and Amorphous Materials", 2nd Edn (Wiley, New York, 1974) pp. 618-704.
3. M. G. GEE and E. A. ALMOND, *Mater. Sci. Technol.* **4** (1988) 655-662.
4. *Idem.*, *Mater. Sci. and Technol.* **4** (1988) 877-884.
5. A. D. KRAWITZ, *Mater. Sci. Eng.* **75** (1985) 29-36.
6. I. CUTTER and R. McPHERSON, *J. Amer. Ceram. Soc.* **56** (1973) 266-269.
7. D. LEWIS and E. J. WHEELER, *J. Mater. Sci.* **4** (1969) 681-684.
8. J. D. SNOW and A. H. HEUER, *J. Amer. Ceram. Soc.* **56** (1973) 153-157.
9. J. CASTAING, J. CADOZ and S. H. KIRBY, *ibid.* **64** (1981) 504-511.
10. R. M. CANNON, "Structure and Properties of Magnesia and Alumina Ceramics; Advances in Ceramics", Vol. 10, (American Ceramic Society, Columbus, Ohio, 1984) pp. 818-838.
11. R. P. STEIN, *J. Appl. Phys.* **32** (1961) 1951-1958.
12. N. WALLBRIDGE, D. DOWSON and E. W. ROBERTS, "Wear of Materials", (ASME, New York, 1983) pp. 202-211.
13. C. S. YUST and F. J. CARIGNAN, *Trans. ASLE* **28** (1984) 245-252.

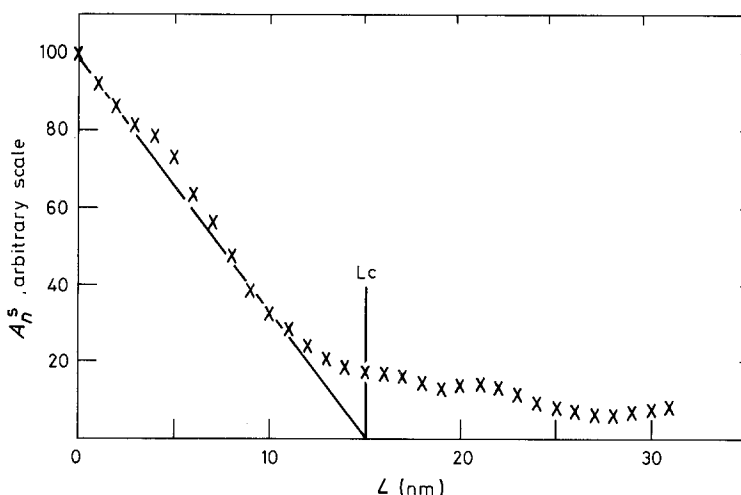


Figure 17 Typical plot of A_n^5 against length parameter L . Crystallite size L_c is given by $A_n^5 = 0$ intercept.

14. Y. ENOMOTO, K. YAMANAKA and K. SAITO, *Wear* **110** (1986) 239-250.
15. I. CUTTER and R. McPHERSON, *Phil. Mag.* **20** (1969) 489-494.
16. *Idem.*, *Wear* **71** (1981) 255-258.
17. R. L. AGHAN and R. McPHERSON, *J. Amer. Ceram. Soc.* **56** (1973) 46-47.
18. S. B. TOH and R. McPHERSON, "Deformation of Ceramics II", *Mater. Sci. Res.* Vol. 18, (Plenum, New York) pp. 723-732.
19. E. BREVAL, J. BREZNAK and N. H. MacMILLAN, *J. Mater. Sci.* **21** (1986) 931-935.

*Received 5 September 1988
and accepted 24 February 1989*